Draft version February 1, 2008
Preprint typeset using LaTeX style emulateapj v. 11/12/01

THE ORIGIN OF ANGULAR MOMENTUM IN DARK MATTER HALOS

Maya Vitvitska[1], Anatoly A. Klypin[1], Andrey V. Kravstov[2], Risa H. Wechsler[3,4], Joel R. Primack[3], & James S. Bullock[5]

Draft version February 1, 2008

ABSTRACT

We propose a new explanation for the origin of angular momentum in galaxies and their dark halos, in which the halos obtain their spin through the cumulative acquisition of angular momentum from satellite accretion. In our model, the build-up of angular momentum is a random walk process associated with the mass assembly history of the halo's major progenitor. We assume no correlation between the angular momenta of accreted objects. The main role of tidal torques in this approach is to produce the random tangential velocities of merging satellites. Using the extended Press-Schechter approximation, we calculate the growth of mass, angular momentum, and spin parameter λ for many halos. Our random walk model reproduces the key features of the angular momentum of halos found in ΛCDM N-body simulations: a log-normal distribution in λ with an average of $\langle\lambda\rangle \approx 0.045$ and dispersion $\sigma_\lambda = 0.56$, independent of mass and redshift. The evolution of the spin parameter in individual halos in this model is quite different from the steady increase with time of angular momentum in the tidal torque picture. We find both in N-body simulations and in our random walk model that the value of λ changes significantly with time for a halo's major progenitor. It typically has a sharp increase due to major mergers, and a steady decline during periods of gradual accretion of small satellites. The model predicts that on average the λ of $\sim 10^{12}\mathrm{M}_\odot$ halos which had major mergers after redshift $z = 3$ should be substantially larger than the λ of those which did not. Perhaps surprisingly, this suggests that halos that host later-forming elliptical galaxies should rotate faster than halos of spiral galaxies.

Subject headings: cosmology: theory — cosmology: dark matter — galaxies: evolution — galaxies: interaction

1. INTRODUCTION

Angular momentum is among the most important quantities determining the size and shape of galaxies, and yet a detailed understanding of its origins remains a missing ingredient in the theory of galaxy formation. Hoyle (1949) was apparently the first astrophysicist who discussed the source of galaxy rotation in the framework of a theory of gravitational instability. He explained galaxy rotation as arising from gravitational coupling with the surrounding matter. Alternative theories of the origin of galaxy rotation due to primordial turbulence and vorticity were also discussed at that time (Wieszacker 1951; Gamow 1952), but such theories were subsequently ruled out by the fact that velocities not arising from gravitation decay in an expanding universe, and also because of improving constraints on velocities derived from cosmic microwave background anisotropies.

Hierarchical clustering of cold dark matter (CDM) (Blumenthal et al. 1984) is now widely believed to describe the origin of structure in the universe, and in this scheme the angular momentum of dark matter halos — and eventually the rotation of galaxies — is usually thought to be produced by gravitational tidal torques in the course of the growth of rotation-free initial perturbations. This is a well-developed (Peebles 1969; Doroshkevich 1970; White 1984) and widely accepted theory, and there is little doubt that the tidal torques mechanism is connected with the generation of angular momentum. To some degree the model is supported by N-body cosmological simulations. For example, if one considers all the mass which at $z = 0$ ends up inside a given halo, then the angular momentum of that mass typically increases linearly with time at early stages of the collapse, just as predicted by the tidal torque theory (e.g., Barnes & Efstathiou 1987). At later times, again in agreement with predictions, the growth in angular momentum slows down (Sugerman et al. 2000).

However, existing models and approximations that try to implement the tidal torque scenario do not agree in detail with the results of fully nonlinear N-body simulations. The predicted angular momentum of halos in the tidal torque model is typically overestimated by a factor of ~ 3 compared to the results of simulations, with a large scatter of the same magnitude (Barnes & Efstathiou 1987; Sugerman et al. 2000). This over-prediction factor can be lessened if one assumes that the angular momentum stops its growth earlier than the turnaround moment (Porciani et al. 2002) because of nonlinear effects, but the scatter still remains very large. The direction of the spin parameter predicted by the theory also has large errors. Lee & Pen (2000) give the average error in the direction of the spin of about 57^o, which agrees with Porciani et al. (2002) who find a mean misalignment of 52^o with a scatter $\sim 35^o$. The source of the errors is still under debate, but it seems that the main effect is due to nonlinear effects which are

[1] Astronomy Department, New Mexico State University, Box 30001, Department 4500, Las Cruces, NM 88003
[2] Department of Astronomy & Astrophysics, University of Chicago, 5640 South Ellis Ave., Chicago, IL 60637
[3] Department of Physics, University of California, Santa Cruz, CA 95064
[4] present address: Department of Physics, University of Michigan, Ann Arbor, MI 48109
[5] Department of Astronomy, The Ohio State University, 140 West 18th Ave., Columbus, OH 43210

difficult to take into account in the tidal torque model (Porciani et al. 2002).

We also address another limitation of the tidal torque picture: predictions for the spin parameter in this framework are for *all* the matter which at $z = 0$ is found in a given halo. At high redshifts this mass is of course not in a single halo. In other words, the tidal torque theory does not predict the rotation of any particular progenitor of the halo in question. In this paper, we will pursue an alternative approach, that of tracing the evolution of the angular momentum of the most massive progenitor of the present-day halo. This alternative approach is much more useful for semi-analytic modeling of galaxy evolution (e.g. Somerville & Primack 1999).

The angular momentum can be expressed in terms of the dimensionless spin parameter, which is defined as

$$\lambda \equiv \frac{J|E|^{1/2}}{GM^{5/2}}. \quad (1)$$

Here J is the angular momentum, E is the total energy, and M is the mass of a halo. The value of the spin parameter roughly corresponds to the ratio of the angular momentum of an object to that needed for rotational support (e.g., Padmanabhan 1993). For example, a spin parameter of $\lambda = 0.05$ implies very little systematic rotation and negligible rotational support. Typical values of the spin parameter of individual halos in simulations are 0.02 to 0.11 (Barnes & Efstathiou 1987; Ryden 1988; Warren et al. 1992; Steinmetz & Bartelmann 1995; Cole & Lacey 1996; Gardner 2001). The distribution of spin parameters in N-body simulations is well described by the log normal distribution:

$$p(\lambda)d\lambda = \frac{1}{\sigma_\lambda\sqrt{2\pi}}\exp\left(-\frac{\ln^2(\lambda/\bar{\lambda})}{2\sigma_\lambda^2}\right)\frac{d\lambda}{\lambda}. \quad (2)$$

The parameters for the log-normal distribution were found to be $0.03 \leq \overline{\lambda} \leq 0.05$ and $0.5 \leq \sigma_\lambda \leq 0.7$ for standard CDM and various variants (e.g. Warren et al. 1992; Gardner 2001). For the ΛCDM cosmology with matter density $\Omega_0 = 0.3$, $\Omega_\Lambda = 0.7$, $h = 0.7$, and $\sigma_8 = 1$, the log-normal parameters were found to be $\overline{\lambda} = 0.042 \pm 0.006$ and $\sigma_\lambda = 0.50 \pm 0.04$ (Bullock et al. 2001b). Note that the $\bar{\lambda}$ parameter of the log-normal distribution (2) is not equal to the mean of λ; rather, $\langle\lambda\rangle \approx 1.078\bar{\lambda}$ for $\sigma_\lambda = 0.5 - 0.6$.

In order to study the evolution of the angular momentum of a dark matter halo it is important to find correlations of the spin parameter with other parameters of the halo and with its environment. Correlation in the directions of spins of nearby halos or galaxies is interesting as an indicator of the strength of large-scale correlations and how much the next infalling satellite "knows" about the previous one. Because the tidal torques are due to perturbations in the gravitational potential, one naively expects that there are long range correlations in spins of halos and, consequently, in the angular momenta of galaxies. Indeed, there are claims that such correlations exist in both observational data and in N-body simulations. But the correlations of galactic rotation axes are measured to be small. If $\hat{L}(\mathbf{x})$ is a unit vector in the direction of the spin axis, then Pen, Lee, & Seljak (2000) find that the correlation function of directions $\langle\hat{L}(\mathbf{x}) \cdot \hat{L}(\mathbf{x}+\mathbf{r})\rangle$ is less than 0.05 for distances $\lesssim 3\ h^{-1}$Mpc, and is even smaller at larger distances. Even at small separations the effect is small and is consistent with no correlations. Results of N-body simulations also indicate that spin correlations are weak at best (Barnes & Efstathiou 1987). Lee & Pen (2000, 2001) found the spin-spin correlation function of halos is ≈ 0.05. Porciani et al. (2002) found no correlation at distances larger than $1h^{-1}$Mpc at late stages of evolution ($z = 0$). These very small correlations also suggest that material which is accreted by a growing halo has very little memory: accretion is mostly random.

The spin parameter of halos in N-body simulations appears to be a very stable statistic and has been shown to be independent of most physical parameters. No dependence has been found on the cosmological model (Barnes & Efstathiou 1987; Warren et al. 1992; Gardner 2001; Lemson & Kauffmann 1999), on halo environment or on halo mass (Lemson & Kauffmann 1999). The only correlation that has been shown to exist is with the time of the last major merger: halos that experienced a recent merger have larger spin (Gardner 2001).

In this paper we investigate the amount of angular momentum that is brought in by the random uncorrelated accretion of satellites. Because there is no systematic rotation of the incoming satellites, one might naively expect that their contribution to the rotation of the accreting object will be small. But at the same time, each act of accretion contributes a large orbital angular momentum. Thus the halo typically acquires a substantial rotation from each large merger, which may later be diluted by many uncorrelated small mergers. The outcome of the process was not obvious in advance, and to our surprise we found that the resulting rotation is quite significant.

We begin, in §2, with an analysis of N-body simulations. There are two reasons for this. First, we study the spin histories of several N-body halos in order to provide a comparative test for our model predictions. Second, we need to characterize the distributions of velocities and angular momenta of infalling satellites, because these are essential inputs for our model.

In §3 we present our random walk model for the build-up of angular momentum in halos. Results of the random walk approximation are presented in §4. We discuss our results and the general implications of our model in §5.

2. SPIN PARAMETERS, HALOS, AND ANGULAR MOMENTA OF SATELLITES IN N-BODY SIMULATIONS

2.1. *Numerical simulations*

We use three N-body simulations of a low-density flat ΛCDM model with the following parameters: $\Omega_0 = 0.3$, $\Omega_\Lambda = 0.7$, and $h = 0.7$. The simulations were done with the Adaptive Refinement Tree (ART) code (Kravtsov et al. 1997).

The first simulation, Klypin et al. (2001), was done only for three halos, but the resolution was extremely high: the mass per particle was $1.2 \times 10^6 h^{-1}\mathrm{M}_\odot$ and the (formal) force resolution was $100h^{-1}$pc. Here we used the power spectrum normalization $\sigma_8 = 0.9$. At redshift $z = 0$ the three halos had virial masses $(1.1 - 1.5) \times 10^{12}h^{-1}\mathrm{M}_\odot$, corresponding to $\sim 10^6$ particles per halo.

In order to find statistics of velocities and orbital angular momenta of satellites needed for the random walk model, we used two additional simulations, which do not have as high resolution as the first one but have many

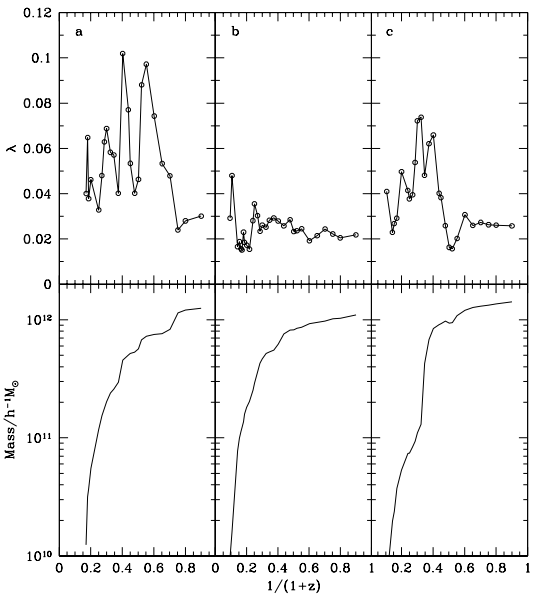

FIG. 1.— Three examples of evolution tracks of galaxy-size halos in N-body simulations. All halos show fast mass growth at high redshifts. At that epoch their spin parameters behaved very violently, but subsequently they mostly declined as the halo masses grew.

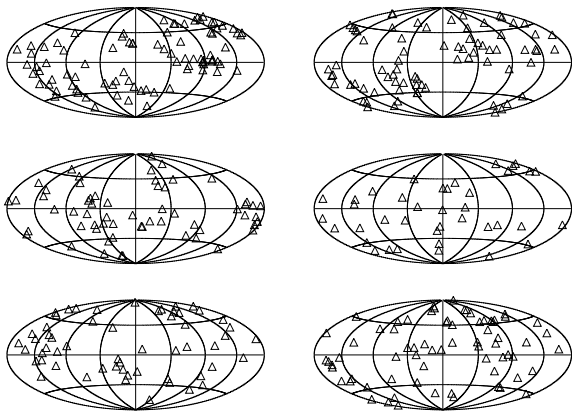

FIG. 2.— The distribution of directions of the orbital angular momenta of accreted satellites relative to the direction of rotation of the central galaxy-sized halos. From top to bottom each row corresponds to halos a, b, and c. Left column is for halos at $z = 1$; the right column is for $z = 0$. The angular momentum of the central halo corresponds to the northern pole (the top point in each panel). There is no clear correlation of the distribution of the directions of satellites either with redshift or with the direction of rotation of the central halo.

more halos. One simulation used 256^3 dark matter particles within a cubic box of comoving size $60h^{-1}$Mpc with mass per particle $m_p = 1.1 \times 10^9 h^{-1} h^{-1} \mathrm{M}_\odot$ and with a (formal) force resolution $1.8h^{-1}$kpc. For this simulation we used $\sigma_8 = 1.0$. This simulation has 15500 dark matter halos at redshift $z = 0$ with masses from $2 \times 10^{10} h^{-1} \mathrm{M}_\odot$ to $\sim 10^{15} h^{-1} \mathrm{M}_\odot$. Another simulation used 512^3 dark matter particles within a cubic box of comoving size $80h^{-1}$Mpc. The mass per particle was $m_p = 3.2 \times 10^8 h^{-1} h^{-1} \mathrm{M}_\odot$. This simulation was run only to $z = 3$. It had 62,000 halos with mass larger than $1.3 \times 10^{10} h^{-1} \mathrm{M}_\odot$. This simulation was used to study statistics of large mergers.

In our simulations the halos are identified by the Bounded-Density-Maxima (BDM) algorithm (Klypin & Holtzman 1997). For distinct halos (halos that are not inside larger halos) the algorithm defines halos as spherical objects with average virial overdensity. Halos inside larger halos are defined as gravitationally bound lumps of dark matter.

2.2. *Evolution of halo spin parameters of major progenitors*

Figure 1 shows the evolution of the mass and the spin parameter of the major progenitors of our three $\sim 10^{12} h^{-1} \mathrm{M}_\odot$ high resolution halos. The spin parameter of the halos clearly changes with time. Even for the most "quiet" halo b the spin parameter changed by a factor 1.5 since redshift 3. For the other two halos the change was even larger. Note that there is no steady increase of the spin with time; instead, there are large sudden changes in λ, which clearly correlate with jumps in the masses of the halos mostly associated with large mergers. The jumps in λ are of both signs: most large merger events are associated with large spin increases, but halo a had a relatively large merger event at $z \approx 0.33$, which decreased its spin by about a factor of two. There is also a tendency of λ to decline during periods of gradual mass accumulation, which is clearly observed in halos b and c at later stages of evolution.

The halos accrete satellites from all directions. Figure 2 shows directions of orbital angular momenta of satellites which are being accreted by the halos at two redshifts. We show satellites that at a given redshift are found in a spherical shell radius between 0.9 and 1.1 times the virial radius. Only satellites that move toward the center are considered. The distribution is not totally random: the satellite spins are clustered. This clustering of orbital spins comes from real-space clustering: there are larger satellites that are surrounded by smaller ones. When a group of satellites falls in to the central halo, they have almost the same angular momentum.

Besides the clustering, there is no discernible pattern in the directions of the satellites. For example, halo b at $z = 0$ has a hole around the northern pole (direction of rotation of the central halo). This would indicate that orbits of satellites are far from the plane of rotation of the central halo. At the same time, halo c has an excess of satellites with the same direction of orbital motion.

These three halos were chosen to reside in a ~ 10 Mpc filament bordering a large void. This is done to roughly mimic the environment of the Local Group. The filament appeared at very high redshifts. The three halos were

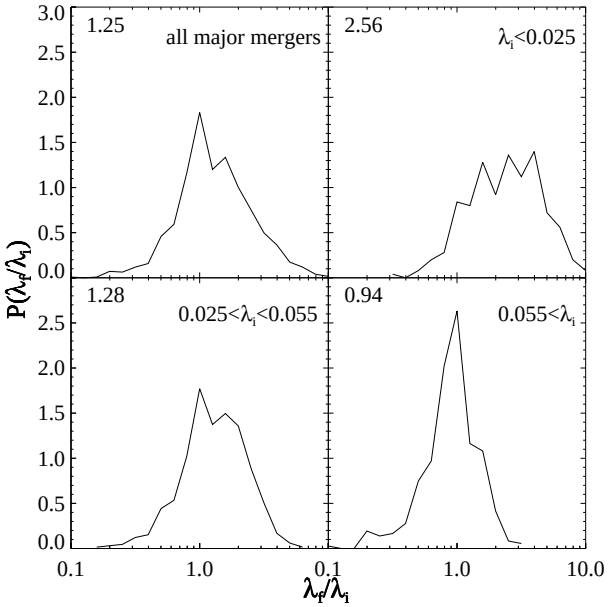

FIG. 3.— Probability distribution of the ratio of final to initial spin parameter λ'_f/λ'_i between subsequent stored time-steps, for halos with $M_{\rm vir} > 5 \times 10^{11} h^{-1} {\rm M}_\odot$ at $z = 0$ that have undergone a major merger. Here λ'_i is the spin parameter λ' at the last stored time-step before the merger, and λ'_f is the spin parameter at the next stored time-step. Panels represent: top left, all halos; top right, $\lambda'_i < 0.025$; bottom left, $0.025 < \lambda'_i < 0.055$; bottom right, $\lambda'_i > 0.055$. The median value of λ'_f/λ'_i is printed in the upper left corner of each plot. Halos with low initial spin parameters typically have large increases in spin in a major merger.

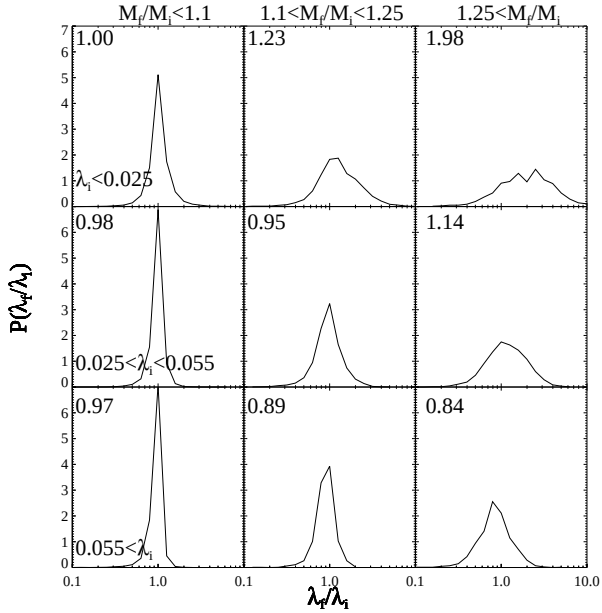

FIG. 4.— Probability distribution of λ'_f/λ'_i for halos with $M_{\rm vir} > 5 \times 10^{11} h^{-1} {\rm M}_\odot$ at $z = 0$. The various panels correspond to halos with different initial spin parameters and different mass ratios. The rows correspond to increasing initial spin values from top to bottom: $\lambda'_i < 0.025$, $0.025 < \lambda'_i < 0.055$, and $\lambda'_i > 0.055$. The columns correspond to increasing mass ratios from left to right: $M_f/M_i < 1.1$, $1.1 < M_f/M_i < 1.25$, and $M_f/M_i > 1.25$, where M_f is the mass of the halo in the later time-step and M_i is the mass of that halo's most massive progenitor in the earlier time-step. The median value of λ'_f/λ'_i is printed in the upper left corner of each panel.

always in the filament, growing by merging with smaller halos. A simple naive expectation is to see a lump of satellites in panels in Figure 2. Its direction would indicate the direction of the filament and the rotation of the halo relative to the filament. We do not find this: there is no obvious large single lump in the diagrams. The problem with the naive expectation is that one imagines a thin tube with the halo inside it. Even qualitatively this is a wrong picture. The filament is much wider (1-2 Mpc) than the virial radii of the three halos ($\sim$ 200 kpc). When the satellites eventually fall in to the halo, they come from different directions in the filament, not from the main axis of the filament. Because of the finite thickness of the filament, one may even expect to find anti-correlation of orbital spins of satellites. Satellites moving parallel to the axis bring opposite signs of the angular momentum when they move above or below the axis.

Figure 2 also shows that there is almost no correlation with redshift for the same halo. Patterns are not reproduced with time. Statistical analysis of the directions confirms our visual impression. The measured distribution is consistent with an uncorrelated random distribution. The data still allow some degree of correlation or anti-correlation because of the small number of satellites and consequent statistical uncertainties. The total number of satellites in our simulations was large, about 300 per central halo at the end of evolution, yet the number of satellites in a shell around the virial radius was much smaller, about 40 for each halo. With the total number of 120 satellites, statistical uncertainties still allow correlation or anti-correlation on the level of 10-20%. Altogether, the evolution of the spin parameter and the directions of accreted satellites indicate that the accumulation of the angular momentum happens mostly in a random, uncorrelated fashion.

We used the second simulation with a large sample of halos to study the correlations of jumps in λ and in mass. The analyses presented here are based on a new structural catalog of halos from this simulation, developed as part of the study of the relationship of the structure of halos to their merging history in Wechsler (2001) and Wechsler et al. (2002), where further details can be found. Briefly, all separate bound virialized halos with more than 20 particles are cataloged at each of 36 stored time-steps from this simulation, and NFW fits (Navarro, Frenk, & White 1996, 1997) are obtained for all halos with more than 200 particles. These catalogs were then compared in order to determine the merging histories of all halos. The statistics presented here are for distinct halos, i.e. those which are not subhalos of another halo.

The simulations indicate that spin parameters of individual halos change very substantially during the growth of halos: there are sharp increases in λ which correlate with periods of fast mass increase, while periods of slow mass increase tend to correlate with declines in the spin parameter. Thus the features illustrated for three halos in Figure 1 are in fact quite general. In Figure 3 we present statistics of the change in the spin parameter in major

mergers, while Figure 4 includes these statistics for a range of changes in the mass of the most massive progenitor. In these figures, we actually plot the changes not in λ but rather in λ', defined as (Bullock et al. 2001b; Dekel et al. 2001)

$$\lambda^{'} = \frac{J}{\sqrt{2}M_{\rm vir}V_cR_{\rm vir}}, \quad (3)$$

where $V_c^2 = GM_{\rm vir}/R_{\rm vir}$ is the circular velocity at the virial radius, $R_{\rm vir}$, for a halo with virial mass $M_{\rm vir}$ (see §3.1 for more details). The spin parameters λ' and λ are approximately equal for typical NFW halos (Bullock et al. 2001b), but λ' is easier to measure in simulations.

For Figure 3 we identified all halos with two progenitors of mass ratio $m/M > 1/3$ in the previous stored time-step, and investigate the distribution of λ'_f/λ'_i in these merging events. On average, we find that λ' increases by about 25% in major merger events (Figure 3, upper left panel), though there is a wide distribution. Not surprisingly, the change in λ' is more severe for cases in which the initial λ' was low; in these cases an incoming satellite is likely to increase the spin regardless of its impact parameter. Halos which have low initial spin values can thus experience jumps of up to a factor of ten in a single merging event. When the initial spin is high, however, merger events can serve to decrease the angular momentum if they come in at opposite direction to the spin. For very high initial values, λ'_f/λ'_i decreases slightly on average, occasionally as much as a factor of five.

Major mergers are clearly important since they can bring in a large amount of angular momentum at once, but minor mergers also play a large role in influencing halo spin. In Figure 4, we show the distribution of λ'_f/λ'_i for a variety of initial spin parameters and changes in halo mass. We see that the spin of halos with very low initial spin values is likely to increase with any incoming material, even a small amount. For halos with intermediate initial spin values, only major mergers are going to have a large effect on their spins, and for halos with very large initial spin values, any incoming mass is likely to decrease the spin. Thus although major mergers produce the largest jumps in λ', we find that the entire mass accretion history is important for its evolution.

2.3. *Velocities and angular momenta of satellites*

In this section we study the infall velocities of satellites into larger halos in the simulations in order to provide inputs to the random walk model. We show that the distribution of infall velocities can be well parameterized by a characteristic Gaussian velocity dispersion and a radial anisotropy parameter. In addition, we find that the velocity anisotropy changes as a function of the mass ratio of satellite to major progenitor, m/M: large satellites tend have more radial orbits. Since we would like to include at least the basic trend with m/M in our model, we make the following simplified division: major mergers satisfy $m/M > 1/3$ and minor mergers satisfy $m/M < 1/3$. We characterize the velocity ellipsoids of each of these populations separately. We sorted all halos by mass and selected pairs of halos starting with the most massive ones. Because we are interested in studying satellites at the time of accretion, we selected only pairs separated by approximately the virial radius R_{vir} of the larger halo in each pair. Three criteria were used: (1) the distance between a pair of halos was required to be $(1 \pm 0.2)R_{\rm vir}$, (2) the relative velocity of halos had to be less than $2V_c$, where V_c is the maximum circular velocity of the larger halo, and (3) the halos had to have negative relative radial velocities (corresponding to inward motion), i.e. the angle between the line from the smaller to the larger halo and their relative velocity vector should be between 0^o and 90^o.

The large sample of halos in our $60h^{-1}$Mpc simulation allows us to study the statistics of relative velocities and angular momenta of satellites falling onto larger halos. We did so by averaging results for expansion factors $a = 0.972, 0.982$, and 1.00. Numerical effects — force and mass resolution and specifics of our halo finder — result in a rather complicated selection of mergers of different mass ratios. The limited force and mass resolution result in destruction of most of satellites of small halos. This is the so called overmerging problem. Because of this problem the galaxy-size halos in this simulation can not be used for studies of minor mergers, since their satellites were not resolved. Small subhalos were resolved for large groups and clusters, which had dozens or hundreds of them (Colin et al. 1999). Thus, we studied minor mergers for "host" halos with masses larger than $10^{14}h^{-1}{\rm M}_\odot$. Overall, there were 543 satellites at radius (1 ± 0.2) of the virial radius of the "host" of which 301 were falling onto the "host" and the rest were moving out. Merging with large satellites was studied mostly at high redshifts. This was done using the $60h^{-1}$Mpc simulation at $z = 1$ and $z = 3$. We also used the $80h^{-1}$Mpc simulation at $z = 3$ to probe statistics of satellites with different masses.

Figure 5 shows several statistics for the minor mergers in our catalog. The upper right panel shows the distribution of infall angles, ϕ, of the smaller halos, where ϕ is the angle between the velocity and radius vectors of the satellite. The distribution of relative infall velocities in units of V_c of the larger halo is shown in the lower left, and the distribution of the relative specific angular momenta of satellites is shown in the bottom right, plotted in units of $L_{\rm vir} = V_cR_{\rm vir}$ of the larger halo, where $L \equiv |\mathbf{r} \times \mathbf{V}|$. The error bars represent Poisson errors.

In the top left panel we show the distribution of the relative velocity as a function of ϕ. There is a small bias in the distribution of velocity vs. angle, with higher infalling velocities corresponding to more radial infall directions. The distribution of the angles in the top right panel shows that there are more infalling halos with radial than with tangential motions.

In general, the magnitudes of the infall velocities are distributed around the circular velocity of the massive progenitor (bottom left panel). The distribution of the velocity can be fit with a 3D Maxwell-Boltzmann distribution ($\sigma_v = 0.62V_c$, $\langle V^2 \rangle = 3\sigma_v^2$):

$$p(V) = \sqrt{\frac{2}{\pi}}\frac{V^2}{\sigma_v^3}\exp(-V^2/2\sigma_v^2). \quad (4)$$

This fit provides a rough characterization of the distribution, but does not fully capture its nature. This is likely because the the velocities are anisotropic, and the Maxwell-Boltzmann distribution describes a system with isotropic velocities. The distribution of satellite angular momenta (bottom right panel), or, equivalently, tangential

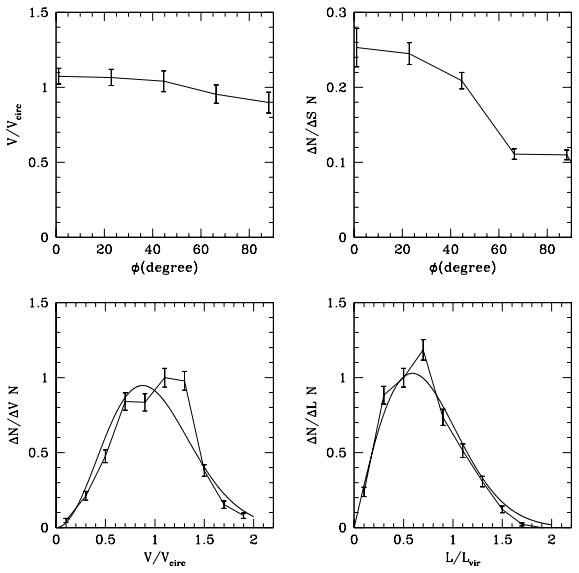

FIG. 5.— The distributions of the angles, velocities, and orbital angular momenta of infalling satellites for minor mergers identified in the simulation. The angle ϕ represents the angle between the radius and velocity vectors. The top right panel shows the distribution of ϕ, and the top left panel shows the distribution with respect to ϕ of the infall velocity in units of the virial circular velocity of the larger halo. The bottom panels show the distributions of the relative velocities (left) and of the angular momenta (right). The error bars show the Poisson errors. Smooth curves are the fits of the distributions (see text for details).

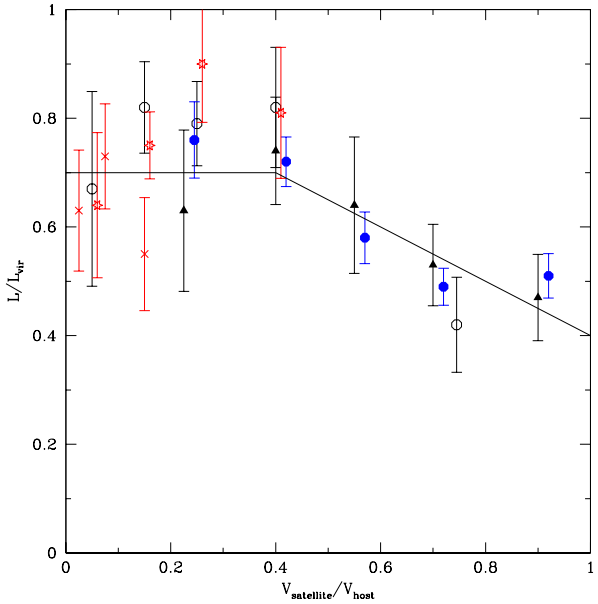

FIG. 6.— The dependence of the specific angular momentum L of a satellite on the ratio of the satellite maximum circular velocity to the maximum circular velocity of the host halo. The specific angular momentum is measured in units of $L_{\rm vir} = R_{\rm vir}V_{\rm vir}$. The specific angular momentum of small satellites is larger than that of large ones; the line shows the fit of eq. (7). There is no dependence on the redshift. Different markers show results for different simulations and redshifts. Stars, open circles, and triangles are for the $60h^{-1}$Mpc simulation at redshifts z =0, 1, and 3 respectively. Crosses are for the three high resolution halos at $z = 0$. Solid circles are for $z = 3$ halos in the $80h^{-1}$Mpc simulation.

velocities, is described reasonably well by a (2D) Maxwell-Boltzmann shape:

$$p(L) = \frac{L}{\sigma^2}\exp(-L^2/2\sigma_L^2), \qquad (5)$$

with $\sigma_L = 0.59L_{\rm vir}$, $\langle L^2\rangle = 2\sigma_L^2$. A good fit is obtained because the tangential velocities are fairly isotropic.

These results suggest that the velocities of satellites are well-described by a 3D Gaussian distribution with a substantial radial velocity anisotropy. We further have checked the distribution of each component of velocity and found them to be roughly Gaussian. Based on this, it is justified to summarize the velocity distribution of infalling satellites with two parameters defining a velocity ellipsoid, one describing the velocity anisotropy,

$$\beta = 1 - \frac{\sigma_\perp^2}{2\sigma_r^2}, \qquad (6)$$

and the other describing the radial Gaussian velocity dispersion, σ_r. For example, in the case of isotropic orbits $\sigma_\perp^2 = 2\sigma_r^2$ and $\beta = 0$, and in the case of nearly radial orbits $\sigma_\perp^2 \ll 2\sigma_r^2$ and $\beta \approx 1$.

From the 60 h^{-1} Mpc numerical simulation, the velocity anisotropy and tangential velocity dispersion were found to depend on the ratio m/M of the mass of the satellite to that of the host galaxy. For major mergers $\beta = 0.8$ and $\sigma_\perp = 0.45V_c$, and for minor mergers $\beta = 0.6$ and $\sigma_\perp = 0.71V_c$. These values are in good agreement with Colin et al. (1999). Note that major mergers are significantly more radial than minor mergers and bring in a factor of 1.6 less specific angular momentum.

We also studied the velocities of satellites in the simulation of the three galaxy-size halos. The statistics of satellites in each halo are much better in this simulation. We can also easily track the evolution of each halo with redshift. The results are consistent with what we found for the larger simulation. For minor mergers the average velocity anisotropy was $\beta = 0.67$ at $z = 0$ and $\beta = 0.53$ at $z = 1$, however, the difference in this value is not statistically significant, and on average the value remains unchanged ($\beta = 0.6$). The three halos in the first simulation have masses of $\sim 10^{12}h^{-1}{\rm M}_\odot$. This is significantly smaller than $10^{13} - 10^{14}h^{-1}{\rm M}_\odot$ in the case of the large-box second simulation where, as we explained above, most of the "satellites" were coming from group-size central halos. Thus, the results for the three halos suggest that there is no (significant) trend of β with the mass of the central halo.

The dependence of the angular momentum of infalling satellites on the mass of the satellites is very important for accurate estimates of the spin parameter λ. We use all available simulations to measure this dependence. Because the mass of a satellite is not always a well defined quantity (e.g., it depends on an uncertain truncation radius and on details of removal of unbound particles), we prefer to use a more reliable characteristic — the maximum circular velocity. Figure 6 shows the dependence of

the specific angular momentum of a satellite L on the ratio of the satellite maximum circular velocity $V_{\rm satellite}$ to the maximum circular velocity of the host halo $V_{\rm host}$. Different markers show results for different simulations and redshifts. Error bars show 1σ shot noise estimates.

Figure 6 indicates that the specific angular momentum of small satellites is larger than that of the large ones. It also shows that there is no dependence of $L/L_{\rm sat}$ on the redshift. The same type of analysis shows that the radial velocity dispersion does not depend on the mass of the satellite: $\sigma_r/V_c = 0.7 \pm 0.1$. Thus, from eq. 6, velocity anisotropy β varies from $\beta = 0.5$ for the small satellites to $\beta = 0.8$ for the major mergers.

We use the following approximation for the rms of the specific angular momentum:

$$L/L_{\rm vir} = \begin{cases} 0.7, & \text{if } V_{\rm sat}/V_{\rm host} < 0.4, \\ 0.9 - 0.5(\frac{V_{\rm sat}}{V_{\rm host}}), & \text{otherwise.} \end{cases} \quad (7)$$

Figure 6 shows that this is a reasonable summary of the simulation data.

3. RANDOM WALK APPROXIMATION

The main idea of our random walk model is that halo angular momentum is built up from the summed contributions of uncorrelated orbital angular momenta of accreted objects during the process of halo assembly. The model needs several ingredients. First, we need to have the mass accretion history for each halo (a merger tree) that tells us how many satellites of what mass are accreted by the major progenitor as a function of redshift. For this, we use the extended Press-Schechter (EPS) approximation (Press & Schechter 1974; Bower 1991; Bond et al. 1991; Lacey & Cole 1993) and the EPS merger-tree method of Somerville & Kolatt (1999). [6] Second, we need to know the position of each satellite at the moment of accretion. The position is assumed to be randomly distributed on a sphere whose radius is the virial radius of the main progenitor, with the main progenitor in the center.

Finally, we need to know the velocities of accreted satellites. The three components of the velocities of each satellite are assumed to be Gaussian, with a velocity anisotropy described by eq. (6). We use $\sigma_r = 0.7V_c$ regardless of the mass of the satellite. The tangential velocity dispersion is assigned in the following way. For a given satellite mass we estimate its concentration parameter (see eqs. (16-17) below). The virial mass and the concentration define the maximum circular velocity $V_{\rm sat}$. We then use eqs. (6-7) to find the tangential velocity dispersion. A realization drawn from the Gaussian distributions gives the three components of the velocity of the satellite.

3.1. *Mass, concentration, and spin parameter*

The model described above provides all of the information needed to calculate the spins of an ensemble of halos. The spin parameter λ is determined by calculating the energy for an NFW halo in virial equilibrium [7] and then using eq. (1). For an NFW halo, $\rho(r) \propto [(r/r_s)(1 + r/r_s)^2]^{-1}$, the virial concentration $c = R_{\rm vir}/r_s$, where the virial radius $R_{\rm vir}$ is defined by the virial mass $M_{\rm vir}$ and by the parameters of the cosmological model:

$$M_{vir} = \frac{4\pi}{3}\rho_{cr}\Omega_0\delta_{th}r_{vir}^3 \quad (8)$$

$$r_{vir} = 443h^{-1}{\rm kpc}\left(\frac{M_{vir}/10^{11}h^{-1}M_\odot}{\Omega_0\delta_{th}}\right)^{1/3}, \quad (9)$$

with (Bryan & Norman 1998)

$$\delta_{th} \simeq (18\pi^2 + 82x - 39x^2)/(1 + x), \quad (10)$$

$$x = -(1 - \Omega_0)a^3/[\Omega_0 + (1 - \Omega_0)a^3], \quad (11)$$

and $a = (1 + z)^{-1}$. In the ΛCDM model $\delta_{th} \sim 180$ at $a \ll 1$ and $\delta_{th} \simeq 340$ at $a = 1$. The total energy of a halo truncated at the virial radius is

$$W = \frac{1}{2}\int \rho(r)\phi(r)\,dr = -\frac{1}{2}\frac{GM_{\rm vir}^2}{R_{\rm vir}}\frac{cg(c)}{f^2(c)}. \quad (12)$$

Here

$$f(c) = \ln(1 + c) - \frac{c}{1 + c} \quad (13)$$

and

$$g(c) = 1 - 2\frac{\ln(1 + c)}{1 + c} - \frac{1}{(1 + c)^2}. \quad (14)$$

The spin is then

$$\lambda = \frac{J}{2V_cM_{\rm vir}R_{\rm vir}}\frac{[cg(c)]^{1/2}}{f(c)}. \quad (15)$$

For the median concentration c, we use the results of Bullock et al. (2001a):

$$c(M_{\rm vir}, z) = \alpha(M_{\rm vir})/(1 + z), \quad (16)$$

$$\alpha(M_{\rm vir}) \simeq 54.8 - 3.34\log(M_{\rm vir}/M_\odot). \quad (17)$$

In this paper we have assumed for simplicity that the halo mass and redshift uniquely determines its concentration. N-body simulations indicate that there is a scatter in c at fixed mass of the order of 35% (Bullock et al. 2001a; Wechsler 2001). In principle, we could include those deviations in our random walk model, but we decided to neglect them because the deviations in λ as a result of this scatter are less than 10 percent. [8]

Thus, knowing the mass and the angular momentum of a halo one can find the halo's concentration and its spin parameter.

3.2. *Random walk model for the angular momentum*

Our main results are derived from two sets of Monte-Carlo merger trees for two different final masses, $M_{\rm max}$. Each set of runs traced the merging history of the most massive progenitor back to $z = 10$ or until its mass fell below $M_{\rm min}$. The first set had $M_{\rm max} = 10^{12}M_\odot$, $M_{\rm min} = 10^8M_\odot$, and a mass resolution (minimum mass of a satellite) of $M_{\rm res} = 10^6M_\odot$. The second set of trees was done with $M_{\rm max} = 10^{15}M_\odot$, $M_{\rm min} = 3 \times 10^8M_\odot$, and $M_{\rm res} = 10^8M_\odot$. We used 300 mass tracks for each set and each track was run 100 times with different realizations of

[6] This method describes fairly accurately the mass accretion history of major progenitors in simulations (Somerville et al. 2000; Wechsler et al. 2002).

[7] Our assumption of virial equilibrium will likely break down just after a major merger occurs. We assume that equilibrium will be restored over a short enough timescale that the general nature of spin evolution will not depend sensitively on this detail.

[8] We also neglect the correlation between concentration and halo merging history (Wechsler 2001; Wechsler et al. 2002).

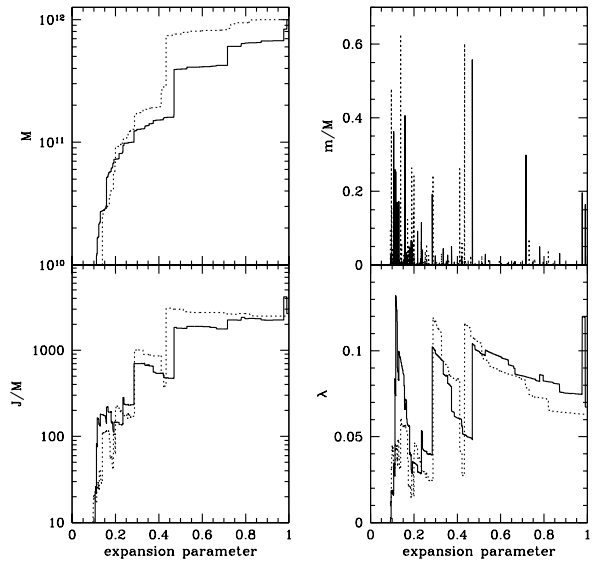

FIG. 7.— The example of two typical evolution tracks (solid and dashed lines) of the two dark matter halos. On the left panels the mass (top) and the specific angular momentum (bottom) are plotted as functions of the expansion parameter $a = (1+z)^{-1}$. The right top panel shows the mass ratio of the most massive merging satellite to the main progenitor, where the case of major merger is defined as mass ratio $m/M \geq 1/3$. The spin parameter as a function of the expansion parameter is plotted in the right bottom panel.

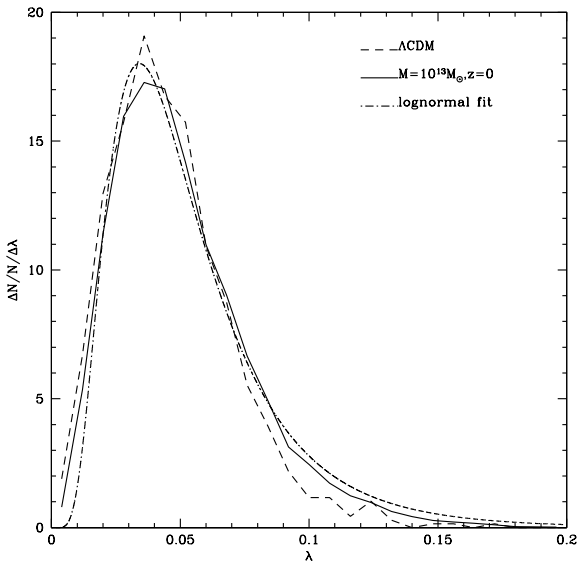

FIG. 8.— Comparison of the distributions of the spin parameter at redshift $z = 0$. The solid line represents the distribution of λ derived using the random walk model. The distribution of λ from our 60 h^{-1} ΛCDM simulation is shown by the dashed curve. The log-normal fit to the random walk model is presented by the dot-dashed curve. The parameters of the log-normal distributions are in Table 1.

satellite velocities. Unless otherwise stated, we use these two sets of merger trees.

The evolution of the mass of two typical $10^{12}M_\odot$ tracks as a function of the expansion parameter is shown on the top left panel in Figure 7. The right top panel shows the ratio of the mass of the biggest satellite to the mass of the main progenitor. The mass of the main progenitor does not change smoothly, because we assume that all new incoming mass instantly merges with the main progenitor.

When the mass of the merging object is significant, there are often dramatic changes in the specific angular momentum (bottom left panel) as well as in the spin parameter (bottom right panel). This also was seen for simulated halos in §2. Of course, major mergers do not always increase the spin parameter; depending on the velocity orientation, such mergers can also decrease the halo's spin. In spite of all these changes in the spins of individual halos, especially in the past when the number of major mergers was significant, we will show below that the *distribution* of the spin parameter doesn't depend on time or on the mass of the main progenitor.

These examples show that the angular momentum doesn't increase linearly. Whether there are increases or decreases in any given merging event depends on the mass of the satellite, its direction of motion, and its velocity. One can also see that at the later stages of the evolution of a dark matter halo, when the mass of the main progenitor doesn't change much, the angular momentum doesn't have dramatic changes either. This behavior is very similar to that found in the N-body simulations, although the comparison cannot be made precise because of the finite differences (up to ~ 0.5 Gyr) between the stored time-steps in the simulation compared to the instantaneous approximation used in our random walk model.

4. RESULTS

4.1. *Comparison with numerical simulations*

We begin by illustrating that our random walk approximation naturally produces a log-normal distribution in λ. Figure 8 shows a comparison between N-body results and our random walk model of spin acquisition. The simulation corresponds to ΛCDM ($\Omega_0 = 0.3$, $h = 0.7$, $\sigma_8 = 1$). For the random walk model we used 200 Monte Carlo merger trees with a final ($z = 0$) mass of the main progenitor $M = 10^{13}M_\odot$. Each mass track was run 100 times with different realizations of satellite velocities. The distribution of the spin parameter from the N-body simulation is shown by dashed line while the distribution from the random walk model is shown by the solid curve. As one can see, there is a reasonably good agreement between the N-body results and the random walk model. To demonstrate that these distributions are well described by the log-normal function we also show a log-normal fit to the random walk data (the dashed-dotted curve). Parameters of the fit are given in Table 1, along with spin parameters measured from N-body simulations.

4.2. *Dependence of the spin parameter on mass and redshift*

As we discussed in §1, N-body simulations indicate that the λ distribution does not vary as a function of redshift or halo mass. Here we test our model against these results.

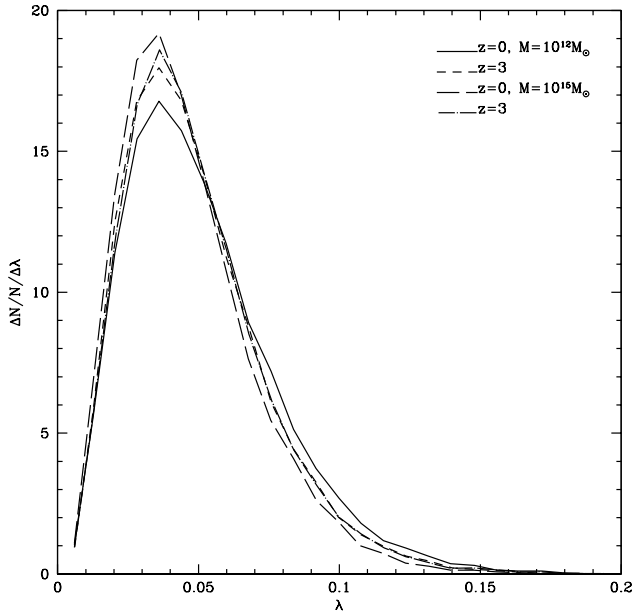

FIG. 9.— The distribution of the spin parameter for halos at z=0 and z=3, for halos whose main progenitor has mass $10^{12}M_\odot$ or $10^{15}M_\odot$ at redshift $z = 0$. The spin distribution has rather weak dependence on mass and redshift.

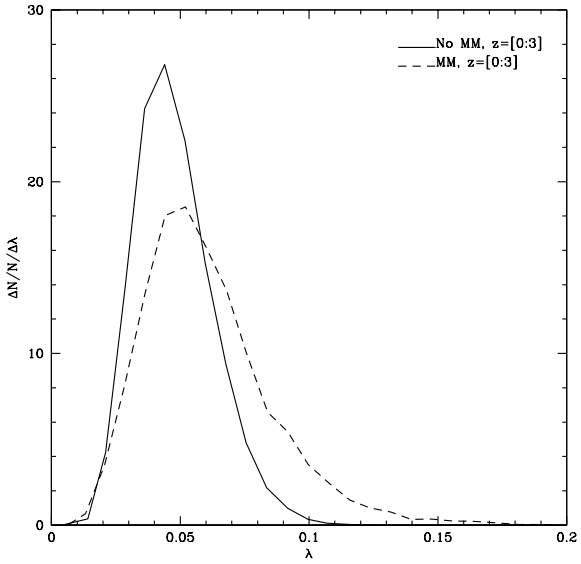

FIG. 10.— The distribution of the spin parameter for dark matter halos that had (dashed line) and didn't have (solid line) a major merger event since redshift $z = 3$. Final mass of the main progenitor at $z = 0$ is $10^{12}M_\odot$. The halos that had major mergers during the last ≈ 11 Gyrs on average have larger (by 25%) spin parameter than those which did not experience a major merger.

We analyzed two different sets of merger trees: one with major progenitor mass $M = 10^{12}M_\odot$ at redshift $z = 0$, and the other with mass $M = 10^{15}M_\odot$ (see §3). For both cases the distributions of the spin parameters were examined at two different redshifts: $z = 0$ and $z = 3$. These are shown in Figure 9. The spin parameter distributions derived from the random walk model show no correlation with either the redshift or the halo mass; the distributions overlap and each has mean value $\langle\lambda\rangle = 0.045$.

4.3. *Major mergers and the spin parameter*

As was just shown, the spin parameter distribution doesn't depend on the redshift or on the mass. But Figure 7 indicates that λ of individual halos in the random walk model is sensitive to whether they have recently had major mergers, as we found in N-body simulations (Figures 1, 3). In this subsection we study the influence of these types of mergers on the distributions of the spin parameter.

We study the effect of major mergers on the distribution of the spin parameter by splitting all halos into two groups: the halos that didn't have any major mergers in the past roughly 11 billion years ($0 \leq z \leq 3$), and the halos that did have a major merger during this period. Since major mergers destroy galactic disks and produce spheroidal stellar systems (see e.g. Barnes 1999), while mergers with mass ratio less than 1/10 probably do not (e.g. Walker, Mihos, & Hernquist 1996), and stellar disks are typically up to about 10 Gyr old, only the halos that did not have a major merger since $z \sim 3$ could host mature spiral galaxies. The distributions of λ for these two groups of halos are shown in Figure 10. The mean value of the spin parameter is 0.0465 and 0.0569 for no major mergers and major mergers since $z = 3$ respectively. in other words, recent major mergers increase the spin parameter almost by 25%. Thus, we find the same result that was found in the N-body simulations: the spin parameters are sensitive to major mergers.

5. DISCUSSION

We have presented a new model for the origin of the angular momentum of dark matter halos in which angular momentum is built up in a random walk fashion by mass accretion events. The evolution of halo angular momentum in this picture is quite different from that inferred from the standard tidal torques argument, in which the angular momentum grows steadily at early times and its growth flattens out at late times. Unlike this standard picture, we do not track the angular momentum of *all* matter that is in the present-day halo; we track only the major progenitor of the halo. The evolution of the spin parameter λ of the major progenitor is a random process in which the the value of λ can vary by factors of a few over its history, with a tendency for sharp increases due to major mergers and steady decline during periods of gradual accretion of small satellites. These general properties of evolution, including large fluctuations in λ, are confirmed by N-body simulations.

Our model predicts that the distribution of the spin parameter is well approximated by the log-normal distribution, with mean and dispersion that do not depend on redshift or on the mass of the main progenitor. The model predicts that on average the spin parameters of halos that

TABLE 1
PARAMETERS OF LOG-NORMAL APPROXIMATIONS FOR THE SPIN DISTRIBUTION IN A ΛCDM MODEL.

Model	$\overline{\lambda}$	σ_λ	Comments
Numerical simulations:			
all halos at $z = 0$	0.0445	0.563	Figure 8
halos that had no major merger since $z = 3$	0.034		
halos that had a major merger since $z = 3$	0.044		
Random walk model:			
halos with $M = 10^{13} M_\odot$, $z = 0$	0.0465	0.556	Figure 8
halos with $M = 10^{12} M_\odot$ & $10^{15} M_\odot$, $z = 0$ & $z = 3$	0.0450	0.560	Figure 9 (mean values)
halos that had no major merger since $z = 3$	0.0465	0.333	Figure 10
halos that had a major merger since $z = 3$	0.0569	0.407	Figure 10

had major mergers after redshift $z = 3$ should be considerably larger than the spin parameters of those halos that did not. Perhaps surprisingly, this implies that halos which host later-forming elliptical galaxies should rotate faster than halos of mature spiral galaxies.

There may actually be observational evidence of this. Planetary nebulae in the two elliptical galaxies NGC 5128 (radio continuum source Cen A) (Hui et al. 1995) and NGC 1316 (Fornax A) (Arnaboldi et al. 1998) are rotating rapidly about their minor axes at large radii. The metal-rich globular clusters of NGC 5128 show rotation similar to that of the planetary nebulae. NGC 5128 is regarded as a prototypical remnant of the merger of two disks, and NGC 1316 is also considered a likely remnant of a fairly recent merger. From numerical simulations (Barnes 1992; Hernquist 1993) of mergers between disk galaxies with bulges, one indeed expects the angular momentum of the remnant to be concentrated in the outer regions. Similar studies of the planetary nebulae of other elliptical galaxies such as NGC 4697 detect less evidence of strong rotation (Mendez et al. 2001), and stellar spectra of only a relatively small fraction of elliptical galaxies show strong rotation at large radii (with $v_r/\sigma \gtrsim 1/2$), e.g. NGC 1395 and NGC 1604 (Franx, Illingworth & Heckman 1989). The globular clusters of M87 and a few other giant elliptical galaxies are also rotating rapidly at large radii (Kissler-Patig & Gerhardt 1998; Cohen 2000; Côté et al. 2001). Galaxies like the cD M87 are thought to form from multiple mergers, and simulations of this process predict that while velocity dispersion should dominate in the central regions, rotation can grow to $v_r/\sigma \sim 1$ in outer regions (Weil & Hernquist 1996). Radial velocity measurements for the planetary nebulae and globular cluster systems of nearby elliptical galaxies should become much more feasible with the advent of multi-object spectrographs on 8-meter class telescopes. Once data are available on a larger number of such systems, it will be interesting to see whether the statistics are consistent with predictions of the random walk model for the origin of galaxy rotation that we have proposed here.

Implementation of the random walk model is a rather complicated procedure if one wants to reproduce N-body results with an accuracy better than about 20 percent. It requires measurements of many parameters of halos and satellites (e.g., halo concentrations for different redshifts and merging trees). The most important and, unfortunately, the most uncertain are the parameters of the velocity ellipsoid of accreted satellites for different masses of the satellites. In principle, these parameters could vary as a function of redshift as well. Estimates for the numerous minor mergers seem to be reasonably reliable (see §2.3). Major mergers are rarer and therefore the estimates are more uncertain. Generally we find that the trajectories of mergers with high m/M ratios are more radial than their low m/M counterparts, but it is difficult to measure the parameters of the velocity ellipsoid accurately.

The model assumes that there is no net angular momentum of infalling satellites and that the satellites are accreted in random fashion. This picture is supported by results of N-body simulations (§2.2). Yet the results allow some degree of either correlation or anti-correlation of orbital spins of the satellites. The allowed effects are rather small (less than 10-20%), but they still may be important for accurate predictions of the angular momenta of halos.

Our colleagues Maller, Dekel, & Somerville (2002) have investigated a simplified version of what we call the random walk model for the origin of the angular momentum of dark matter halos, in comparison with a version of the tidal torques model more sophisticated than the standard one discussed briefly in §1 of the present paper. They find that both models can reproduce the log-normal distribution of halo spin parameters seen in simulations, with appropriate tuning of the model parameters. Their work is thus complementary to that presented here.

We expect that our random walk model for the origin of halo angular momentum through the accretion of satellites will be useful both conceptually and practically. In addition to giving a much better fit to the distribution of halo spin parameters than the tidal torque theory, it also accords better with the hierarchical nature of the process by which halos grow in the cold dark matter model. Moreover, because it is based on the same extended Press-Schechter formalism used in semi-analytic approaches and because it is so simple to implement, we expect that it will prove invaluable in improving the treatment of angular momentum in modeling the formation and evolution of galaxies. For these same reasons, it will be worthwhile to test and improve the random walk model.

We conclude with some comments about the implications of our model for disk galaxy formation and the angular momentum problem in disks. This random walk picture is somewhat at odds with the formalism made popular

by Fall & Efstathiou (1980) in which the gas is initially well mixed within a smoothly rotating halo, and subsequently falls in to form an angular momentum supported disk.[9] In our random walk model, the halo angular momentum obtains its smoothly varying distribution through a series of clumpy merger events and subsequent relaxation. Unlike a picture in which tidal torques determine the spin of a halo at very early times, when the gas and dark matter was well-mixed, our scenario would suggest that the angular momentum distribution of gas could be considerably different than that of the dark matter. The merging satellite galaxies are likely to be strongly affected by the tidal field of the central object, and their gas is likely to shock against the gas in and around the host. Since it is known that the angular momentum distribution in dark halos is quite unlike that in disk galaxies (Bullock et al. 2001b; van den Bosch, Burkert, & Swaters 2001), generally with an excess of low-spin material, our random walk picture might provide an interesting avenue for exploring solutions of this angular momentum distribution problem and also of the well-known angular momentum overcooling problem (e.g. Navarro & Steinmetz 1997). Work in this direction is under way.

ACKNOWLEDGMENTS

We acknowledge support from NASA and NSF grants at NMSU, Ohio State, and UCSC, and we thank Avishai Dekel, Tsafrir Kolatt, Ari Maller, and Rachel Somerville for helpful discussions. A.K. is grateful to the Institute of Astronomy at Cambridge for hospitality and financial support during his extended visit to Cambridge University. A.V.K. was supported by NASA through a Hubble Fellowship grant from the Space Telescope Science Institute, which is operated by the Association of Universities for Research in Astronomy, Inc., under NASA contract NAS5-26555

REFERENCES

Arnaboldi, M., et al. 1998, ApJ, 507, 759
Barnes, J.E., & Efstathiou, G. 1987, ApJ, 319, 575
Barnes, J.E. 1992, ApJ, 393, 84
Barnes, J.E. 1999, in ASP Conf. Ser. 187, The Evolution of Galaxies on Cosmological Timescales, ed. J.E. Beckman & T.J. Mahoney (San Francisco: ASP), 293
Blumenthal, G.R., Faber, S.M., Primack, J.R., & Rees, M. 1984, Nature, 311, 517
Blumenthal, G.R., Faber, S.M., Flores, R., & Primack, J.R. 1986, ApJ, 301, 27
Bond, J.R., Cole, S., Efstathiou, G., & Kaiser, N. 1991, ApJ, 379, 440
Bower, R. 1991, MNRAS, 248, 232
Bryan, G.L., & Norman, M.L. 1998, ApJ, 495, 80
Bullock, J.S., Dekel, A., Kolatt, Kravtsov A.V., Klypin, A.A., Porciani, C., & Primack, J.R., 2001b, ApJ, 555, 240
Bullock, J.S., Kolatt, T.S., Sigad, Y., Somerville, R.S., Kravtsov A.V., Klypin, A.A., Primack, J.R., & Dekel, A. 2001a, MNRAS, 321, 559.
Cohen, J.G. 2000, AJ, 119, 162
Cole, S., & Lacey, C. 1996, MNRAS, 281, 716
Colin, P., Klypin, A.A., & Kravtsov A.V, 2000, ApJ, 539, 561
Côté, P., et al. 2001, ApJ, 559, 828
Dekel, A., Bullock, J.S., Porciani, C., Kravtsov, A.V., Kolatt, T.S., Klypin, A.A., & Primack, J.R., 2001, in ASP Conf. Ser. 230, Galaxy Disks and Disk Galaxies (San Francisco: ASP), eds. J.G. Funes, S.J., and E.M. Corsini, astro-ph/0011002
Doroshkevich, A.G. 1970, Astrofizika, 6, 581
Fall, S.M., & Efstathiou, G. 1980, MNRAS, 193, 189
Flores, R., Primack, J.R., Blumenthal, G.R., & Faber, S.M. 1993, ApJ, 412, 443
Franx, M., Illingworth, G.D., & Heckman, T. 1989, ApJ, 344, 613
Gamow, G., 1952, Phys. Rev, 86, 251
Gardner, J.P., 2001, ApJ, 557, 616
Hernquist, L. 1993, ApJ, 409, 548
Hoyle, F., 1949, *Problems of Cosmical Aerodynamics* Dayton: Central Air Documents Office.
Hui, Xiaohui, Ford, H.C., Freeman, K.C., & Dopita, M.A. 1995, ApJ, 449, 592
Kissler-Patig, M., & Gebhardt, K. 1998, AJ, 116, 2237
Klypin, A.A., Holtzman, J., 1997, astro-ph/9712281
Klypin, A.A., Kravtsov, A.V., Bullock, J.S., & Primack, J.R. 2001, ApJ, 554, 903
Kravtsov, A.V., Klypin, A.A., & Khokhlov, A.M., 1997, ApJS, 111, 73
Lacey, C., & Cole, S. 1993, MNRAS, 263, 627
Lee, J., & Pen, U. 2000, ApJ, 532, L5
Lee, J., Pen, & U., 2001, ApJ, 555, 106
Lemson, G., Kauffmann, G. 1999, MNRAS, 302, 111
Maller, A.H., Dekel, A., & Somerville, R.S. 2002, MNRAS, 329, 423
Mendez, R.H., et al. 2001, ApJ, 563, 135
Mo, H.-J., Mao, S., & White, S.D.M. 1998, ApJ, 297, L71; MNRAS, 295, 319
Navarro, J.F., Frenk, C.S., & White, S.D.M. 1996, ApJ, 462, 563
Navarro, J.F., Frenk, C.S., & White, S.D.M. 1997, ApJ, 490, 493
Navarro, J.F., & Steinmetz, M. 1997, ApJ, 478, 13
Padmanabhan, T., 1993, *Structure formation in the universe*, Cambridge: Cambridge Univ. Press
Peebles, P.J.E. 1969, ApJ, 155, 393
Pen, U., Lee, J., & Seljak, U. 2000, ApJ, 543, L107
Porciani, C., Dekel, A., & Hoffman, Y. 2002, MNRAS, 332, 325
Press, W.H., & Schechter, P. 1974, ApJ, 187,425
Ryden, B.S. 1988, ApJ, 329, 589
Somerville, R.S., & Kolatt, T.S. 1999, MNRAS, 305, 1
Somerville, R.S., & Primack, J.R. 1999, MNRAS, 310, 1087
Somerville, R.S., Lemson, L.G., Kolatt, T.S., & Dekel, A. 2000, MNRAS, 316, 479
Steinmetz, M., & Bartelmann, M. 1995, MNRAS, 272, 570
Sugerman, B., Summers, F.J., Kamionkowski, M., 2000, MNRAS, 311,762
van den Bosch, F. 1998, ApJ, 507, 601
van den Bosch, F.C., Burkert A., & Swaters R.A. 2001, MNRAS, 326, 1205
Walker, I.R., Mihos, J.C., & Hernquist, L. 1996, ApJ, 460, 121
Warren, M.S., Quinn, P.J., Salmon, J.K., & Zurek, W.H. 1992, ApJ, 399, 405
Wechsler, R.H. 2001, PhD Dissertation, University of California, Santa Cruz
Wechsler, R.H., Bullock, J.S., Primack, J.R., Kravtsov, A.V., & Dekel, A. 2002, ApJ, 568, 52
Weil, M.L., & Hernquist, L. 1996, ApJ, 460, 101
Wieszacker, C.F. von, 1951, ApJ, 114, 165
White, S.D.M. 1984, ApJ, 286, 38

[9] This picture was further developed by Blumenthal et al. (1986), Flores et al. (1993), and Mo, Mao, & White (1998), who took into account the response of the dark halo to the infalling baryons.